



Efficient localized heating of silver nanoparticles by low-fluence femtosecond laser pulses



H. Huang ^{a,b}, M. Sivayoganathan ^{a,b}, W.W. Duley ^{a,c}, Y. Zhou ^{a,b,*}

^a Centre for Advanced Materials Joining, University of Waterloo, Ontario, N2L 3G1, Canada

^b Department of Mechanical & Mechatronics Engineering, University of Waterloo, Ontario, N2L 3G1, Canada

^c Department of Physics & Astronomy, University of Waterloo, Ontario, N2L 3G1, Canada

ARTICLE INFO

Article history:

Received 20 September 2014

Received in revised form

22 December 2014

Accepted 12 January 2015

Available online 20 January 2015

Keywords:

Femtosecond laser

Localized heating

Localized surface plasmon

ABSTRACT

Highly localized heating can be obtained in plasmonic nanomaterials using laser excitation but the high fluences required often produce unacceptable damage in and near irradiated components and structures. In this work we show that plasmonic nanostructures involving aggregated Ag nanoparticles (Ag NPs) can be heated effectively without attendant damage to the surrounding material when these structures are irradiated with many overlapping femtosecond (fs) laser pulses at very low fluence. Under these conditions, the effectiveness of heating is such that the temperature of 50 nm Ag NPs can be raised to their melting point from room temperature. Aggregates of these NPs are then observed to grow into larger spherical particles as laser heating continues. Imaging of these materials shows that the initiation of melting in individual Ag NPs depends on the local geometry surrounding each NP and on the polarization of the incident laser radiation. Finite difference time domain (FDTD) simulations indicate that melting is triggered by localized surface plasmon (LSP)-induced electric field enhancement at “hotspots”.

© 2015 Elsevier B.V. All rights reserved.

1. Introduction

The control of localized heating on micro- and nanoscales is emerging as a powerful way of manipulating thermally activated processes in medical therapy [1], ultrafast switching of phase-change materials [2], nanowelding [3], and nanoscale chemical interactions [4]. Realization of nanoscale thermal control usually involves the assembly of a nanoscale electro-thermal system consisting of nanowire or nanotubes [3,4]. Currently, this can only be accomplished using expensive and sophisticated devices such as thermal cantilevers, the atomic-force microscope and scanning electron microscopy (SEM). Laser radiation can also be used for nanoscale heating but this requires complex optical systems to achieve the spatial resolution necessary for nanoscale processing [5,6].

Recently, plasmonic nanomaterials or structures have been reported to produce highly localized heat generation under laser irradiation [7–10]. The heating in plasmonic nanomaterials and structures is mainly attributed to the concentration of laser energy

in hotspots where the electric field is enhanced due to localized surface plasmon (LSP) [9,10]. Because the hotspots are localized near the surface of these materials, nanoscale heating utilizing plasmonic nanomaterials and nanostructures is promising. In addition as the generation of hotspots, including the location and amplitude of the electric field enhancement factor, depends on structure geometry together with laser polarization [11,12], the nanoscale laser heating process can be influenced through control of these parameters.

Due to the high intensity in fs laser pulses and their short duration which minimizes heat conduction compared to longer pulse lasers, fs laser irradiation is an efficient way to direct energy to hotspots in plasmonic nanomaterials [13]. In this paper, we show that fs laser irradiation with fluence as low as $\sim 7.2 \text{ mJ/cm}^2$ is effective in the localized heating and melting of individual Ag NPs contained in extended plasmonic nanostructures. This fluence is much lower than that previously reported ($\sim 110 \text{ mJ/cm}^2$) for fs laser irradiation induced melting of Ag nanomaterials [9]. Under these irradiation conditions, there is no apparent damage to Ag NPs surrounding the selected plasmonic structure.

2. Experimental and simulation

Ag NPs with a $\sim 2 \text{ nm}$ thick PVP coating were prepared following the method reported by Peng et al. [14]. Sodium citrate

* Corresponding author: Centre for Advanced Materials Joining, Department of Mechanical & Mechatronics Engineering, University of Waterloo, Ontario, N2L 3G1, Canada.

E-mail address: nzhou@uwaterloo.ca (Y. Zhou).

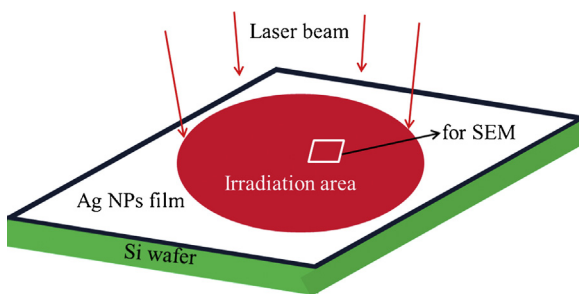


Fig. 1. Schematic of the experimental configuration.

($\text{Na}_3\text{C}_6\text{H}_5\text{O}_7$) aqueous solution (12 ml, 200 mM) was added to 200 ml deionized water with vigorous stirring, followed by adding polyvinylpyrrolidone (PVP, 2 ml, 20 mM), $[\text{Ag}(\text{NH}_3)_2]^+$ (2 ml, 120 mM), and Ag seed (~ 5 nm diameter, 0.4 ml, 1 mM) aqueous solution. Then ascorbic acid ($\text{C}_6\text{H}_8\text{O}_6$) aqueous solution (10 ml, 10 mM) was added drop-wise and the mixed solution was stirred for 30 min. The prepared Ag NPs solution were then centrifuged and re-dispersed into deionized water to eliminate the residual PVP, Ag seed, and other ions in the solution. Ag NPs films with NPs embedded in the PVP matrix were obtained by immersing clean silicon wafers into the re-dispersed Ag NPs solution and keeping them in a dry environment (humidity $\leq 35\%$) to let the water evaporate. Ag NPs films on silica glass were also prepared using a similar method and then used for UV-vis absorption spectroscopic investigation.

The Ag NPs films were irradiated for up to 60 s with fs laser pulses (Coherent Inc., wavelength = 800 nm, pulse duration = 35 fs, repetition rate = 1 kHz) at average fluence (calculated by divide the spot area with the pulse energy) ranging from $\sim 3.6 \text{ mJ/cm}^2$ to 28.8 mJ/cm^2 . The schematic of the experimental setup is shown in Fig. 1. The morphology of the Ag NPs films in the irradiation area before and after laser irradiation was characterized by SEM (LEO 1550) and transmission electron microscopy (TEM, JEOL, JEM-2010F). Commercial finite difference time domain (FDTD) software (Lumerical Inc.) was used to simulate the distribution of hotspots and the absorption in plasmonic Ag NPs structures during irradiation with 800 nm laser light.

3. Results and discussions

The SEM images of Ag NPs film morphology before and after laser irradiation are shown in Fig. 2. Due to the nature of the deposition process, these films had a non-uniform thickness distribution. At their thickest point, the films contained ~ 6 layers of Ag NPs. Fig. 2a–b shows that, before irradiation, most of the individual NPs in these films had sizes between 20 and 80 nm with an average size of 50 nm. Individual NPs were irregularly shaped as shown in the inset in Fig. 2a. After irradiation for 10 s (10,000 pulses), at a fs laser fluence of $\sim 7.2 \text{ mJ/cm}^2$ some spherical particles were generated, as indicated by the dashed circles in the inset image in Fig. 1c. The size distribution of these newly formed spherical particles, averaged over 300 particles, is given in Fig. 2d. It can be seen that large spherical particles having diameters between 80 and 160 nm appear after 10 s laser irradiation. Particles in this size range were not present before irradiation. The generation of larger spherical particles suggests that fs laser irradiation under these conditions produced efficient heating which caused the melting and subsequent coalescence of the original Ag NPs. Molecular dynamic simulations and experimental observations of the solid-state sintering behavior of NPs [15,16] has shown that sintered NPs will not grow into larger sphere-like structures until the sintering temperature approaches the melting point. No apparent change was observed in either the morphology or size distribution

of these generated spherical particles when the irradiation time was increased to 30 and 60 s. As shown in Fig. 3, the size of the large spherical particles is still in the 80–160 nm range after the NP film was irradiated at a fluence of $\sim 7.2 \text{ mJ/cm}^2$ for 30 s (Fig. 3a and b) and 60 s (Fig. 3c and d). This indicates that the generation of spherical particles does not depend on the irradiation time and implies that other factors such as laser fluence and the localized structure in the NP film may dominate the interaction.

Fig. 4 shows SEM images of the morphology in Ag NPs film irradiated at different fluences for 10 s. At 28.8 mJ/cm^2 (Fig. 4a), the NPs in the irradiated film were melted and sintered due to the large energy input, and the Si wafer shows the development of small holes (see the arrows in Fig. 4b). These holes are the result of ablation. Since this fluence is much smaller than the damage threshold in Si (170 mJ/cm^2) irradiated with a 25 fs pulse [17], hole drilling in the Si wafer can be attributed to an enhancement in the local laser intensity as a result of multiple scattering [18]. At a laser fluence of $\sim 14.4 \text{ mJ/cm}^2$, spherical particles are also obtained and the size distribution of these spherical particles is almost the same as that in samples irradiated at a fluence of $\sim 7.2 \text{ mJ/cm}^2$. The only exception is that a few slightly larger (160–220 nm) particles are also generated (Fig. 4c and d). When the laser fluence was decreased to 3.6 mJ/cm^2 (Fig. 4e), modification was not evident in the irradiated NP films. These observations indicate that the generation of spherical particles is influenced by the laser fluence, but there is no direct correlation between laser fluence and the resulting size of the spherical particles.

Enhancement in the local laser intensity due to multiple scattering, including speckle formation and sub-wavelength self-focusing [18], was first considered as the origin of efficient heat generation leading to the melting of Ag NPs and formation of larger size spherical particles. This might be expected to be important in multiple-layer Ag NP films. For example, sub-wavelength self-focusing of an incident laser beam was observed at the bottom surface of a multiple layer ZnO NP film [18]. The laser intensity in the self-focused beam was enhanced by a factor of 2.5. In the present experiments, the enhancement factor was estimated to be ~ 6 . This value was obtained from the ratio of the fluence ($\sim 28.8 \text{ mJ/cm}^2$) consistent with producing visible damage to the Si substrate in the present experiments to that reported as the damage threshold (170 mJ/cm^2) for irradiation of Si with a 25 fs pulse [17]. Based on this comparison, we conclude that sub-wavelength self-focusing is not the primary source of the efficient heating and melting of NPs found in the present experiments [13].

To minimize the influence of sub-wavelength self-focusing, and to investigate the underlying causes of efficient fs laser induced localized heating, single-layer Ag NPs films were prepared and irradiated under the same conditions. Fig. 5 shows SEM images of the morphology of single-layer NPs films before and after 16 laser pulses, which was the minimum number of overlapping pulses needed to produce an observable change in the single layer Ag NP film. These images show that larger spherical NPs can also be generated in single-layer NPs films after fs laser irradiation (as indicated by arrows in Fig. 5b). This implies that multiple scattering induced sub-wavelength self-focusing is not the source of the efficient heating effect resulting in melting of the original NPs. SEM observations in the same area of the NPs film before (Fig. 5a) and after (Fig. 5b) fs laser irradiation show that a large spherical particle has been created in the structure where 4 NPs were located (ring 1 in Fig. 5a and b). This particle is shown in the inset image in Fig. 5b. Removal of NPs from the PVP matrix leaves and outline of their original positions (e.g. ring 2 in Fig. 5b). The inset image in Fig. 5b indicates that 3 of the 4 adjacent Ag NPs coalesce into a larger particle while the remaining NP was unaffected. This suggests that selective fs laser induced heating of Ag NPs is concentrated in certain

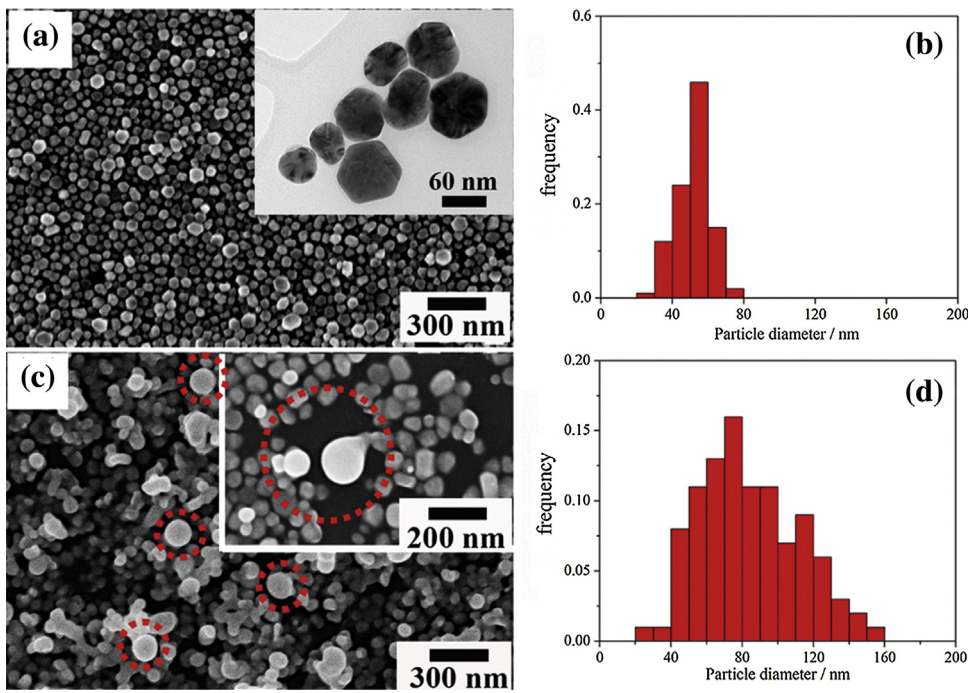


Fig. 2. SEM and TEM images of morphology for Ag NPs films on a Si wafer before and after irradiation, (a) SEM image of NP film before irradiation, the inset TEM image shows the details of the NPs; (b) Size distribution of the NPs in the film before irradiation; (c) SEM image of NP film after irradiation at a fluence 7.2 mJ/cm^2 for 10 s (10,000 pulses), the inset image shows the formation of larger spherical nanoparticles; (d) Size distribution of the spherical particles in the film after irradiation.

structures where the absorption of laser pulse energy is enhanced, and that this heating occurs without apparent damage to the NPs surrounding these structures. This is consistent with the observation that spherical particles with diameters of ~ 76 , 83 and 100 nm are located close to structures in which 3 , 4 and 7 NPs were absent after laser irradiation (dashed rings in Fig. 5c and e, respectively).

The number of Ag NPs removed was estimated from the SEM images (Fig. 5). The area, S , of the removed structure is $S = (1/\alpha)n\pi R^2$ where α is the filling factor for the NPs in the structure, n is the number of NPs, and $R = 25 \text{ nm}$ is the average NP radius. Volumes calculated for the resulting spherical particles correspond almost exactly to the sum of the volumes of the particles removed from the PVP matrix.

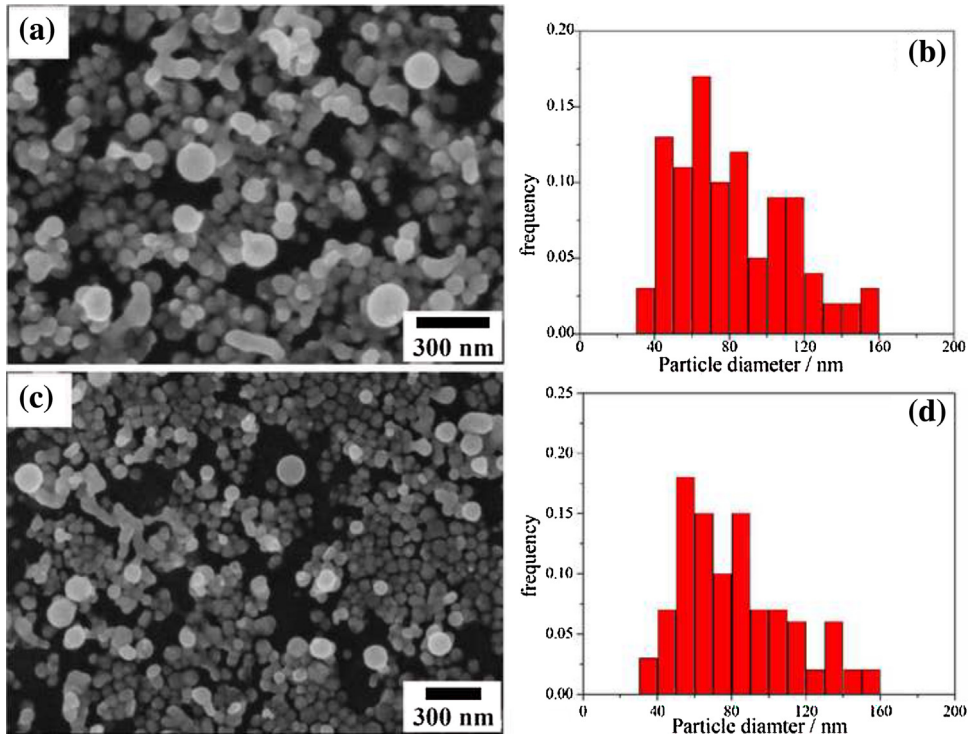


Fig. 3. Morphology and size distribution as determined from SEM imaging of spherical particles in NP films after fs laser irradiation at a fluence of $\sim 7.2 \text{ mJ/cm}^2$. (a and b) 30 s exposure, (c and d) 60 s exposure.

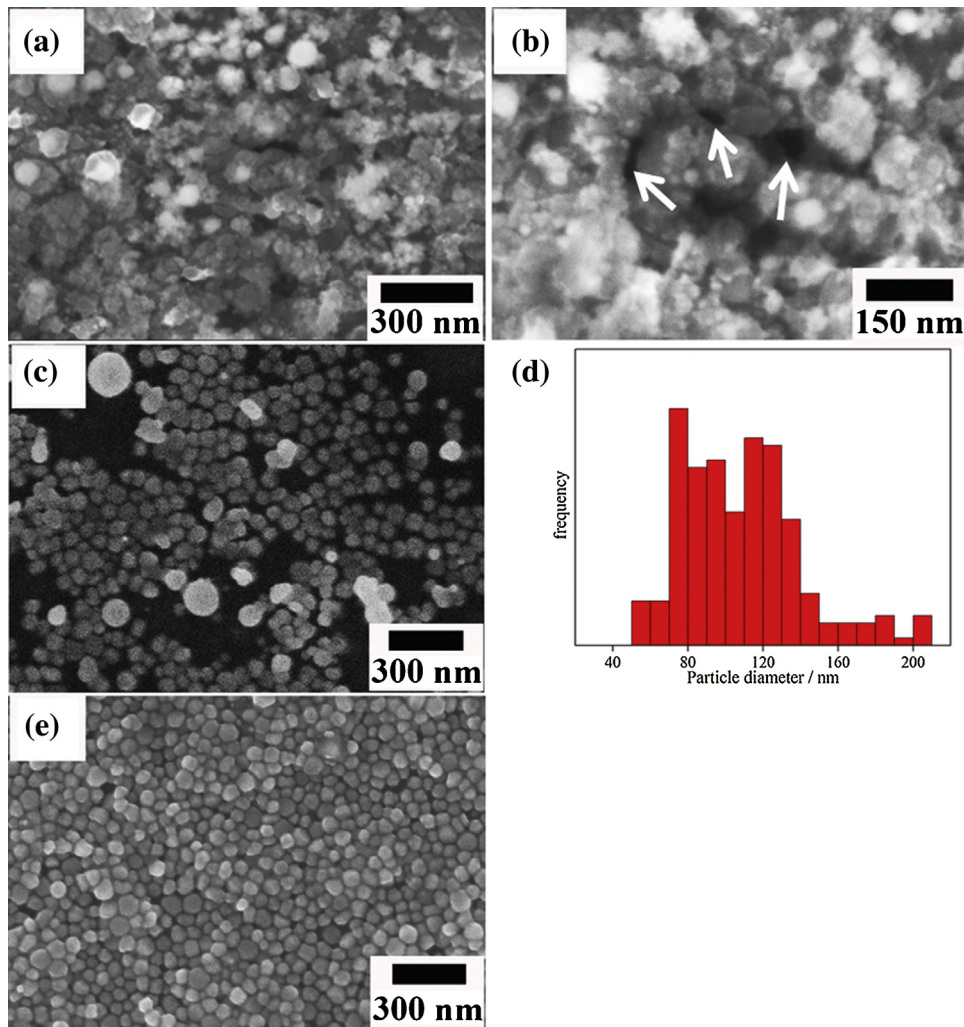


Fig. 4. SEM images of the morphology and size distribution of spherical particles generated in NP films following fs irradiation for 10 s at different fluences. (a and b) 28.8 mJ/cm², (c and d) 14.4 mJ/cm², (e) 3.6 mJ/cm².

The removal of NPs is likely due to fs laser irradiation induced ablation of the NPs and/or the PVP shell around these particles [19–21]. It should be noted that ions/electrons produced in the initial stages of the ablation process can increase the absorption of fs laser energy [22,23], leading to enhanced heating of the NPs.

Another characteristic of the laser interaction is that Ag NP dimers whose long axis is parallel to the direction of laser polarization (as indicated by the double ended arrows in Fig. 6) tend to be removed from the PVP matrix. Individual isolated NPs are not removed under these conditions (Figs. 5b–e and 6). This effect, and the dependence on laser polarization and local structure are similar to the polarization-dependent generation of LSP-induced hotspots which enhances the local electric field. This suggests that the efficient heating of NPs in these films can be attributed to LSP-induced hotspots.

FDTD simulations have been carried out to identify the location of hotspots in Ag NP structures containing 2, 3, 4 and 7 NPs as indicated by the SEM observations (Fig. 5), and to study the effect of LSP-induced hotspots on the heating of NPs and the formation larger spherical particles in specific structures. Aggregates containing 5 and 6 NPs are not considered, because they are not close-packed structures and are rarely seen in the Ag NP films. A schematic of the simulation geometry is shown in Fig. 7a, where

Ag NPs are supported on a Si wafer with 2 nm thick oxide layer. For simplification, all the NPs were taken to be spherical with a diameter of 50 nm and irradiation occurs in air. The gap distance between adjacent NPs was set to the $8(\pm 2)$ nm which was an average value of gap distance obtained from 200 measurements using SEM images. The distribution of the E^2 field component in the XY plane at the half height of the NP is recorded in the simulations. Fig. 7 shows the calculated hotspot distribution in a variety of structures. These are indicated by the bright red and yellow regions, while the bold dark red rings outline the NPs. It is evident (Fig. 7b) that the maximum enhancement (~ 10) in the quadratic electric field, E^2 , in the hotspots in single NPs occurs in the direction of the laser polarization. The same enhancement (~ 10) is seen in an Ag NP dimer when the laser polarization is perpendicular to the long axis (Fig. 7c). The low electric field enhancement in these hotspots is consistent with reduced laser induced heating and emission of electrons and ions from the NPs and the PVP shell, and with the observation that isolated single NPs or NPs dimers with their long axis perpendicular to the laser polarization direction were not removed from the irradiated PVP matrix (Fig. 6). The simulations indicate that the field enhancement (~ 40) is much greater in Ag NP dimers with their long axis parallel to the direction of laser polarization (Fig. 7d). As proposed by Xu et al. [24], the effect of this enhancement is to cause the NPs to move towards each

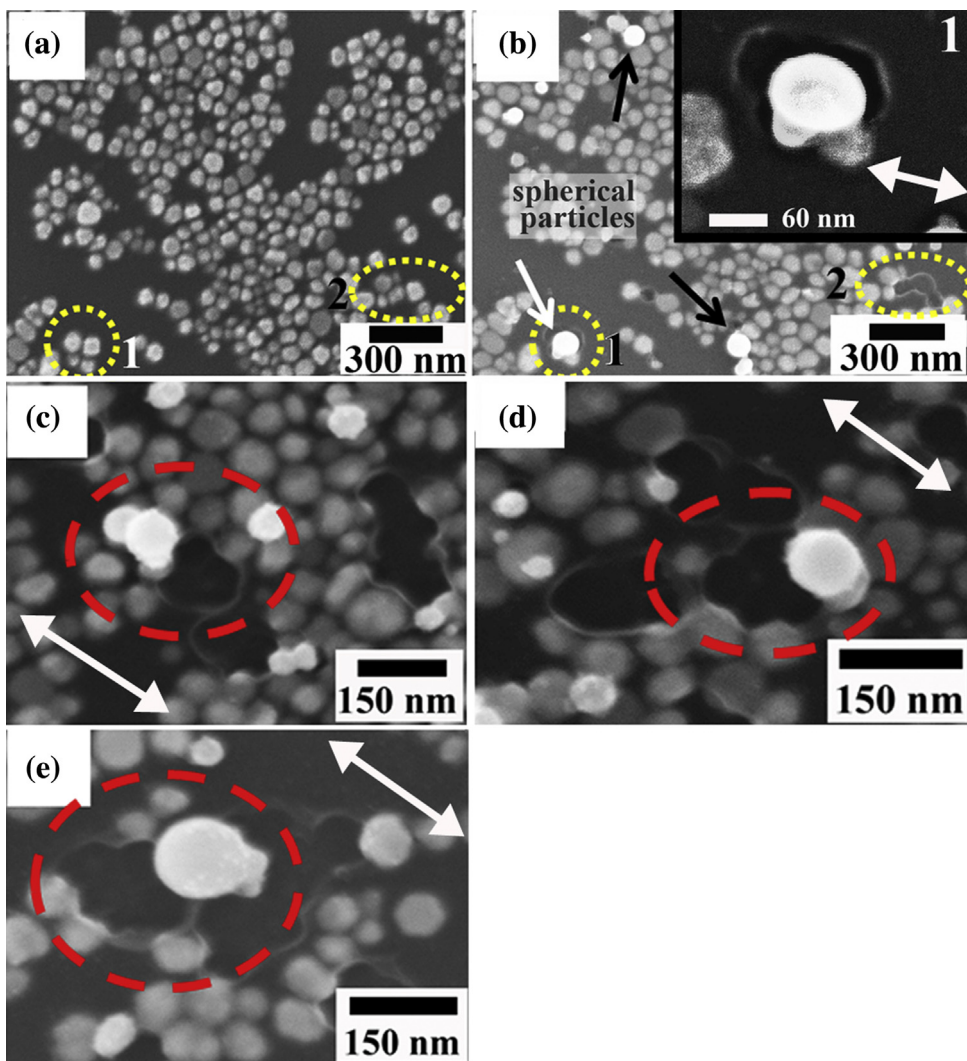


Fig. 5. SEM images of the morphology for single layer NP films before and after irradiation with 16 fs laser pulses at 7.2 mJ/cm^2 . (a) Before irradiation; (b) After irradiation of film in (a). The arrows show the generation of spherical particles while the double-ended arrow in the inset image shows the direction of the laser polarization. The dashed rings 1 and 2 show the area where NPs were ejected, and the inset image shows a magnified view of the circular area 1; (c, d, e) Spherical particles generated near NP assemblies containing 3, 4 and 7 NPs. The double ends arrows show the direction of laser polarization.

other. The attractive force is shown with single ended arrows in Fig. 7. This attraction facilitates the coalescence of NPs and initiates the formation of larger spherical particles. The electric field enhancement and the proposed movement of the NPs in other structures are shown in Fig. 7e–g.

To determine how the presence of hotspots may contribute to the efficient heating of NPs via enhanced laser energy absorption, we estimate the minimum absorption efficiency, Q_{abs} , that must be achieved to melt Ag NPs using equations where $Q_{\text{abs}} = E_{\text{abs}}/E_{\text{inc}}$ and $E_{\text{abs}} = n [(4/3)\pi R^3 \rho (C \Delta T + H_m)]$. $E_{\text{inc}} = FA$ is the total laser energy incident on the structure, where $F = 72 \text{ J/m}^2$ is the laser fluence and A is the effective absorption area of the structures as outlined in Fig. 7. E_{abs} is the energy required to completely melt the Ag NPs in a structure containing n NPs, while R is the NP radius, ρ is the density, C is the heat capacity, and H_m is the latent heat of fusion. Taking $R = 25 \text{ nm}$ for an Ag NP, $\rho = 1.0 \times 10^4 \text{ kg/m}^3$, $C = 230 \text{ J/kg}^\circ\text{C}$ and $H_m = 1.05 \times 10^5 \text{ J/kg}$, we find that the minimum absorption efficiency, Q_{abs} , required to produce melting ($\Delta T = 940^\circ\text{C}$) in these structures is >0.7 . The maximum temperature that the particle can reach is estimated to be $\sim 993^\circ\text{C}$ if all the incident laser radiation is absorbed. Depression of the melting temperature is not

considered here because this is not significant for 50 nm Ag NPs [25,26]. High absorption efficiencies for NPs as calculated here are usually only obtained when the LSP of the structure is in resonance with the incident laser polarization and wavelength [27]. However,

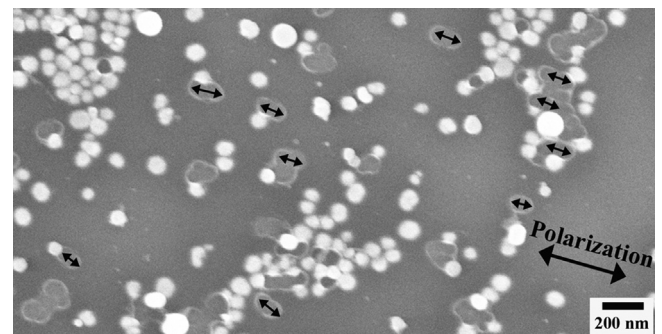


Fig. 6. Laser polarization dependent ejection of NP dimers in a single layer NP film after irradiated by 16 fs laser pulses at a fluence of 7.2 mJ/cm^2 . The double ended arrows show the long axis of the NP dimer.

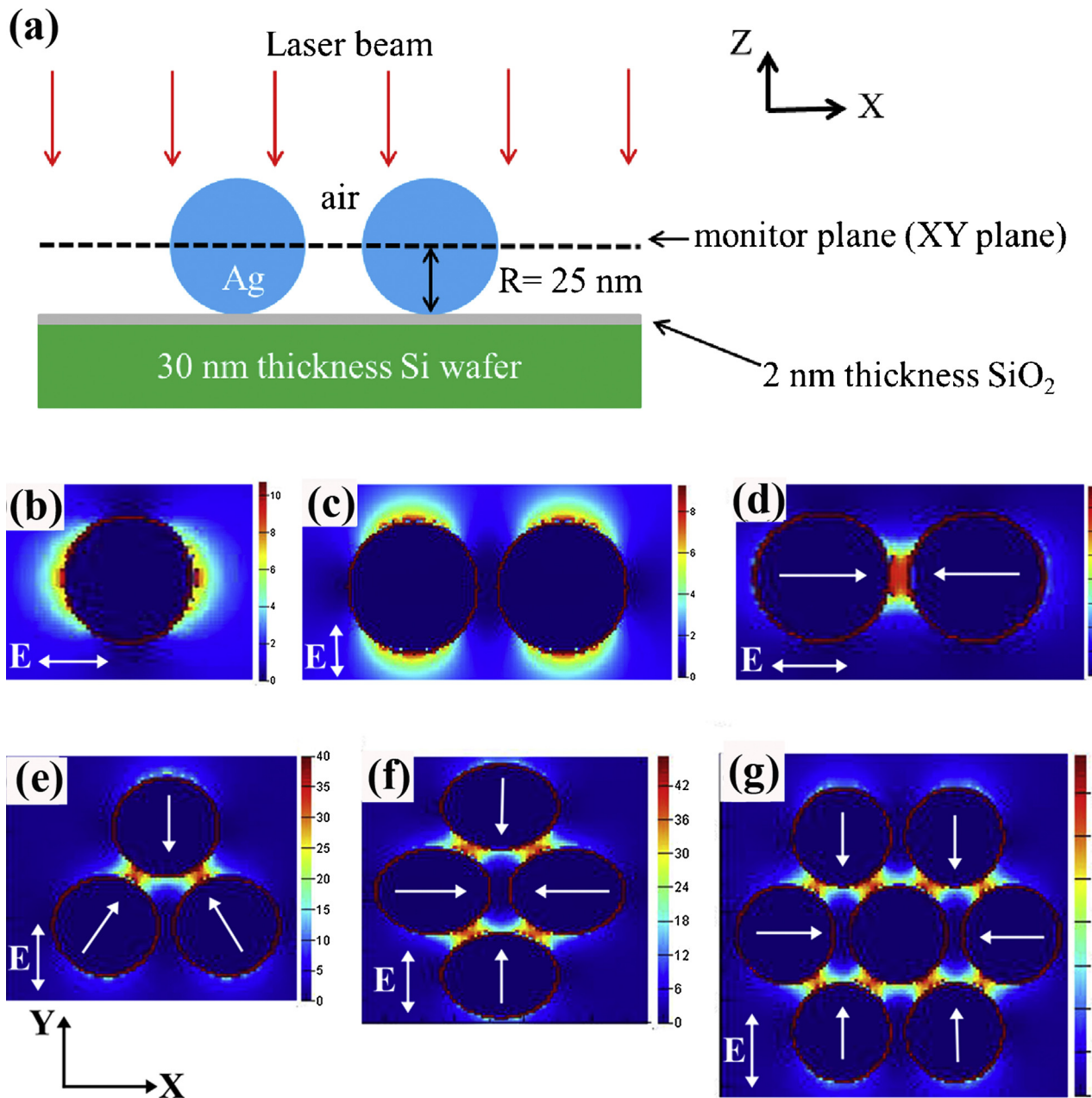


Fig. 7. Simulated quadratic electric field (E^2) distribution in Ag NPs structures assembled from 50 nm NPs. (a) Schematic of simulation setup, a dimer structure is taken as an example; (b–g) Hotspots distribution in Ag NPs structures with different number of particles. The hotspots are located in the bright red and blue area. The double-end arrows show the electric field direction of the incident laser. The single-end arrows show the proposed motion of NPs. The gap between the NPs is set to be the measured average distance of 8 nm.

the measured absorption spectrum (Fig. 8) clearly shows that no resonance occurs at 800 nm in the Ag NP structures at low incident intensity. This is also supported by the calculated absorption spectrum based on the FDTD simulation (inset in Fig. 8). Some differences between the experimental and calculated spectrum are observed at wavelengths near 550 nm. This difference likely arises because the NPs in the simulation were assumed to be spherical and embedded in air, while in reality the NPs are irregular and are coated with a ~2 nm thick PVP layer. The temperature rise in individual NPs is estimated in the usual way based on the measured absorbance ($=0.1$ at 800 nm wavelength). Then $0.1 = \ln(I_0/I)$ where I_0 is the incident light intensity and I is the intensity of the light after passing through the NP film. The measurements show that the absorption efficiency is <0.1 which is much smaller than the

minimum absorption efficiency ~ 0.7 required to produce melting. As a result, the temperature rise of the NPs is $<140^\circ\text{C}$ which is much lower than the melting temperature of Ag. This shows that the observed efficient heating and melting of Ag NPs is not primarily due to the LSP resonance itself, but likely occurs because of enhanced absorption arising from increased excitation of ions and electrons produced from the decomposition of PVP on the surface of Ag NPs in the vicinity of hotspots as reported previously [22,23,28]. However, the generation of the LSPs is important in the initial stages of the laser NP interaction, as LSP induced hotspots act to facilitate and enhance coupling of fs radiation into these structures. Additional laboratory and theoretical studies are needed to better understand the origin of the absorption enhancement in these systems.

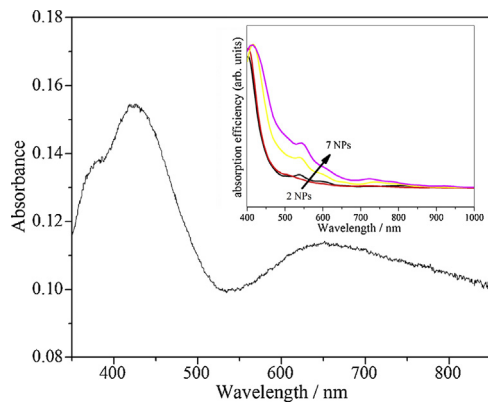


Fig. 8. Measured absorbance of Ag NPs film, the inset image is the calculated absorption spectrum of the structures containing 2, 3, 4, 7 NPs.

4. Conclusions

In this work, we show that Ag NPs in specific symmetric plasmonic structures can be efficiently heated up to their melting point when irradiated with very low fs laser fluence ($\sim 7.2 \text{ mJ/cm}^2$). Enhanced coupling and efficient heating was strongly dependent on the geometry of these NPs structures and laser polarization. This selective heating effect was found to be most evident in clusters of 2, 3, 4 and 7 Ag NPs. FDTD simulations and measured absorption spectra indicate that the efficient heating and melting of NPs in these structures was triggered by LSP-induced hotspots. The overall effect is strongly dependent on the orientation of laser polarization in relation to the symmetry axis of selected structures.

Acknowledgements

The work is financially supported from the National Sciences and Engineering Research Council of Canada (NSERC) and the State Scholarship Fund of China (no. 2011640021). The authors would

like to acknowledge Carmen Andrei, from the Canadian Center of Electron Microscopy at McMaster University which is supported by NSERC and other government agencies, for help in the TEM measurements.

References

- [1] D.O. Lapotko, E. Lukianova, A.A. Oraevsky, Lasers Surg. Med. 38 (2006) 631.
- [2] S.H. Lee, Y. Jung, R. Agarwal, Nat. Nanotechnol. 2 (2007) 626.
- [3] H. Tohyoh, S. Fukui, Phys. Rev. B 80 (2009) 155403.
- [4] C.Y. Jin, Z. Li, R.S. Williams, K.C. Lee, I. Park, Nano Lett. 11 (2011) 4818.
- [5] H.F. Hamann, M. O'Boyle, Y.C. Martin, M. Rooks, H.K. Wickramasinghe, Nat. Mater. 5 (2006) 383.
- [6] C.H. Chu, C.D. Shiu, H.W. Cheng, M.L. Tseng, H.P. Chiang, M. Mansuripur, D.P. Tsai, Opt. Express 18 (2010) 18383.
- [7] I. Alessandri, J. Colloid Interface Sci. 351 (2010) 576.
- [8] G. Baffou, R. Quidant, F.J. Garcia de Abajo, ACS Nano 4 (2010) 709.
- [9] L. Liu, P. Peng, A. Hu, G. Zou, W.W. Duley, Y. Zhou, Appl. Phys. Lett. 102 (2013) 073107.
- [10] V.K. Valev, et al., Adv. Mater. 24 (2012) OP29.
- [11] A. Grubisic, E. Ringe, C.M. Cobley, Y. Xia, L.D. Marks, R.P. Van Duyne, D.J. Nesbitt, Nano Lett. 12 (2012) 4823.
- [12] M. Hu, J. Chen, Z.Y. Li, L. Au, G.V. Hartland, X. Li, M. Marquez, Y. Xia, Chem. Soc. Rev. 35 (2006) 1084.
- [13] H. Huang, L. Liu, P. Peng, A. Hu, W.W. Duley, Y. Zhou, J. Appl. Phys. 112 (2012) 123519.
- [14] P. Peng, A. Hu, Y. Zhou, Appl. Phys. A 108 (2012) 685.
- [15] H.A. Alarifi, M. Aris, C. Ozdogan, A. Hu, M. Yavuz, Y. Zhou, Mater. Trans. 54 (2013) 884.
- [16] W. Widijayastuti, S.Y. Lee, F. Iskandar, K. Okuyama, Adv. Powder Technol. 20 (2009) 318.
- [17] H.O. Jeschke, M.E. Garcia, M. Lenzner, J. Bonse, J. Kruger, W. Kautek, Appl. Surf. Sci. 197–198 (2002) 839.
- [18] J. Park, C. Park, H. Yu, J. Park, S. Han, J. Shin, S.H. Ko, K.T. Nam, Y. Cho, Y. Park, Nat. Photonics 7 (2013) 454.
- [19] A. Plech, V. Kotaidis, M. Lorenc, J. Boneberg, Nat. Phys. 2 (2006) 44.
- [20] A. Gloskovskii, et al., Phys. Rev. B 77 (2008) 195427.
- [21] T. Döppner, T. Fennel, P. Radcliffe, J. Tiggesbäumker, K.H. Meiweis-Broer, Phys. Rev. A 73 (2006) 031202.
- [22] T. Ditmire, R.A. Smith, J.W.G. Tisch, M.H.R. Hutchinson, Phys. Rev. Lett. 78 (1997) 3121.
- [23] M. Kundu, D. Bauer, Phys. Rev. Lett. 96 (2006) 123401.
- [24] H. Xu, M. Kall, Phys. Rev. Lett. 89 (2002) 246802.
- [25] C. Tang, Y.M. Sung, J. Lee, Appl. Phys. Lett. 100 (2012) 201903.
- [26] Q. Jiang, S. Zhang, M. Zhao, Mater. Chem. Phys. 82 (2003) 225.
- [27] F.J. Beck, A. Polman, K.R. Catchpole, J. Appl. Phys. 105 (2009) 114310.
- [28] É. Boulais, R. Lachaine, M. Meunier, Nano Lett. 12 (2012) 4763.